

Nanocarbon-copper thin film as transparent electrode

R. A. Isaacs, H. Zhu, Colin Preston, A. Mansour, M. LeMieux, P. Y. Zavalij, H. M. Iftakhar Jaim, O. Rabin, L. Hu, and L. G. Salamanca-Riba

Citation: [Applied Physics Letters](#) **106**, 193108 (2015); doi: 10.1063/1.4921263

View online: <http://dx.doi.org/10.1063/1.4921263>

View Table of Contents: <http://scitation.aip.org/content/aip/journal/apl/106/19?ver=pdfcov>

Published by the [AIP Publishing](#)

Articles you may be interested in

[Dynamics of laser induced metal nanoparticle and pattern formation](#)

Appl. Phys. Lett. **106**, 061914 (2015); 10.1063/1.4908251

[Ag nanowire percolating network embedded in indium tin oxide nanoparticles for printable transparent conducting electrodes](#)

Appl. Phys. Lett. **104**, 071906 (2014); 10.1063/1.4866007

[Impact of wavelength dependent thermo-elastic laser ablation mechanism on the generation of nanoparticles from thin gold films](#)

Appl. Phys. Lett. **101**, 263107 (2012); 10.1063/1.4773301

[Contact resistance of flexible, transparent carbon nanotube films with metals](#)

Appl. Phys. Lett. **97**, 143116 (2010); 10.1063/1.3496465

[High near-infrared transparency and carrier mobility of Mo doped In₂O₃ thin films for optoelectronics applications](#)

J. Appl. Phys. **106**, 063716 (2009); 10.1063/1.3224946

Want to publish your paper in the
#1 MOST CITED journal in applied physics?

With *Applied Physics Letters*, you can.

AIP | Applied Physics
Letters

THERE'S POWER IN NUMBERS. Reach the world with AIP Publishing.





Nanocarbon-copper thin film as transparent electrode

R. A. Isaacs,¹ H. Zhu,¹ Colin Preston,¹ A. Mansour,² M. LeMieux,¹ P. Y. Zavalij,³
H. M. Iftekhhar Jaim,¹ O. Rabin,^{1,4} L. Hu,^{1,a)} and L. G. Salamanca-Riba^{1,b)}

¹Materials Science and Engineering Department, University of Maryland, College Park, Maryland 20742, USA

²Carderock Division, Naval Surface Warfare Center, West Bethesda, Maryland 20817, USA

³Department of Chemistry and Biochemistry, University of Maryland, College Park, Maryland 20742, USA

⁴Institute for Research in Electronics and Applied Physics, University of Maryland, College Park, Maryland 20742, USA

(Received 18 December 2014; accepted 2 May 2015; published online 14 May 2015)

Researchers seeking to enhance the properties of metals have long pursued incorporating carbon in the metallic host lattice in order to combine the strongly bonded electrons in the metal lattice that yield high ampacity and the free electrons available in carbon nanostructures that give rise to high conductivity. The incorporation of carbon nanostructures into the copper lattice has the potential to improve the current density of copper to meet the ever-increasing demands of nanoelectronic devices. We report on the structure and properties of carbon incorporated in concentrations up to 5 wt. % (~22 at. %) into the crystal structure of copper. Carbon nanoparticles of 5 nm–200 nm in diameter in an interconnecting carbon matrix are formed within the bulk Cu samples. The carbon does not phase separate after subsequent melting and re-solidification despite the absence of a predicted solid solution at such concentrations in the C-Cu binary phase diagram. This material, so-called, Cu covetic, makes deposition of Cu films containing carbon with similar microstructure to the metal possible. Copper covetic films exhibit greater transparency, higher conductivity, and resistance to oxidation than pure copper films of the same thickness, making them a suitable choice for transparent conductors. © 2015 AIP Publishing LLC. [<http://dx.doi.org/10.1063/1.4921263>]

Transparent conductive electrodes are a critical component in optoelectronic applications such as displays, solar cells, and touch screens.¹ Traditionally, transparent conducting metal oxides (TCOs), such as indium tin oxide (ITO), the current commercial standard, and conductive polymers, are used. ITO is brittle and expensive, thus nanostructures, such as nanowires of silver,^{2–5} gold,^{6,7} and copper,^{1,2,8–11} are now being realized with higher performance and better mechanical stability than ITO^{2,12,13} yet potentially with lower material and manufacturing costs. Copper exhibits poor environmental stability particularly at the nanoscale. Core-shell structures or ALD coatings of Cu nanostructures have demonstrated reduced oxidation, but the long term stability of exposed copper does not yet meet the standard for practical applications.^{14,15} "Covetics" are materials formed by the incorporation of high concentrations (~10 wt. %, ~37 at. %) of nanoscale carbon in a metal matrix.¹⁶ We report thin (10–30 nm) Cu covetic films with higher optical transparency and better electronic properties and higher environmental stability than Cu metal films of the same thickness.

Cu (99.99%) was converted to Cu covetic by adding 4 or 5 wt. % C (denoted Cu cv 4% (5%)) by Third Millennium Materials, LLC. The conversion process involves melting the metal and stirring in ~5 wt. % (21.78 at.%) particles of activated carbon with diameter of $\leq 50 \mu\text{m}$ to the liquid metal in the presence of a high DC current.¹⁷ Two deposition techniques were used to make transparent electrodes from Cu

covetic: e-beam deposition and pulsed laser deposition (PLD). For e-beam deposition, bulk Cu cv 5% or pure Cu metal (0% C) was used as the target from which material was transferred into either Si (100) or glass substrate using a Denton e-beam evaporator with a base pressure of $\sim 5 \times 10^{-6}$ Torr. A voltage of 8 kV and a current of 90–130 mA were applied, giving an evaporation rate of 0.2–0.3 nm/s. The substrates were kept at room temperature. Films with thicknesses of 10, 20, and 30 nm were deposited of Cu covetic and Cu (0% C) for comparison. For PLD, bulk Cu cv 4% was used as a target and material transferred into a thin film using a custom-built PLD system (Bluewave Semiconductor, Inc.) equipped with a frequency-doubled Quantel Brilliant B solid-state Nd:YAG pulsed laser (532 nm, 10 Hz, 2.3 W \pm 0.5 W).¹⁸ The chamber has a base pressure of $\sim 1 \times 10^{-6}$ Torr. Evaporation took place in an Ar (99.9999%) atmosphere with ≤ 10 ppb O₂ and ≤ 20 ppb H₂O at a pressure of 100 mTorr and substrate temperature of 150 °C. The rotating target was ablated for 1 min prior to film deposition that lasted 60 min.

Bulk Cu covetic and pure Cu samples were polished for Scanning Electron Microscopy (SEM) and X-ray photoelectron spectroscopy (XPS) in an iterative process using diamond paper starting from 30 μm and ending with 0.5 μm particle size. The samples were then sonicated first in acetone followed by isopropyl alcohol for 5 min each to remove any loose diamond particles that might be left from the polishing procedure. Samples were characterized using a Hitachi SU-70 field emission SEM with an energy dispersive x-ray spectrometer (EDS) Bruker Si drift detector (SDD) and spatial resolution of 1 nm. Lamellas for transmission electron microscopy (TEM) were prepared from the bulk samples by

^{a)}binghu@umd.edu

^{b)}riba@umd.edu

mechanical polishing followed by Ar⁺ ion milling and from the thin film samples by a Helios 550 FIB/SEM. The samples were plasma cleaned prior to TEM observation to remove organic surface contamination using a South Bay PC-2000 Plasma cleaner. TEM observation was carried out in a JEOL 2100F field emission TEM operated at 200 kV with a spherical aberration coefficient of $C_s = 0.5$ mm, point-point resolution of 0.19 nm and lattice resolution of 0.10 nm. X-ray powder diffraction (XRD) was obtained on a Bruker D8 Discover powder diffractometer using CuK_α radiation from a sealed tube, Göbbel mirror with 0.5 mm pinhole collimator, and Vantec500 area detector. Carbon content was estimated from XPS with Mg X-rays (1287 eV) using a Physical Electronics Model 5400 spectrometer. Survey spectra were collected at constant pass energy of 89.5 eV. Multiplex spectra were collected at constant pass energy of 35.8 eV and an electron takeoff angle of 45°. An area of 1.1 mm was analyzed by XPS. Depth profiling was done with 4 keV Ar-ions using a rastered area of 5 mm × 5 mm with an estimated sputtering rate of ~10.2 nm of Cu per minute. A Dimensions 3000 atomic force microscope (AFM) was used to characterize the surface roughness of the films.

Figure 1(a) shows the structure of bulk Cu cv 5%, where lattice structure nanocarbon with a modulation of ~1.6 nm is observed along several crystallographic directions in the sample. The (011)-electron diffraction pattern from the area (Figure 1(b)) presents weak satellite spots (marked by arrows), corresponding to the modulation observed in the high resolution TEM (HRTEM) image in Fig. 1(a). This region of the sample contains a relatively high concentration of carbon of 7.4 ± 0.8 wt. % (29.72 at. %) as measured by EDS (not shown) in the TEM and suggests that the carbon is incorporated into the copper lattice. Other areas of the sample showed lower concentration of C. *In-situ* TEM measurements have shown that it is possible for nucleation of carbon nanostructures to occur from the end faces of metal particles inside larger host tubes when multi-walled nanotubes containing encapsulated Co, Fe, FeCo, and Ni nanowires are irradiated with a strong electron beam.¹⁹ It is thus likely that during the fabrication of covetics, the high electric current applied to the molten metal leads to self-organization, or

self-assembly, of carbon nanostructures within the lattice of the metal.²⁰ XPS sputtering depth profile of a copper covetic sample with nominally 5 wt. % carbon exhibits 3.2 wt. % (15 at. % ± 4 wt. %) (Figure 1(c)). As expected, the XPS data show high carbon at the surface of the sample due to hydrocarbon contamination that tapers off to a consistent level (~15 at. %) within the bulk sample. The carbon content is not uniform throughout the bulk, so variations in the local carbon concentration are not unusual. This value is lower than the nominal 5 wt. % but is in agreement with SEM/EDS spectra (not shown) that measured 3.90 ± 0.8 wt. % (~15.97 at. %).

AFM (not shown) of nominal e-beam deposited Cu cv 5% films on Si (100) using pieces of the bulk Cu cv 5% sample as target shows smooth surfaces, exhibiting an average RMS roughness of only 1 nm which can also be seen in the HRTEM image of Figure 2(a) for an 18 nm thick Cu cv film. The XRD spectrum from this sample shown as inset to Fig. 2(a) exhibits crystalline structure with Cu (111) preferred orientation. The crystalline grains form a columnar structure where the grains extend from the interface with the Si substrate to the film surface. No copper oxide or any of the allotropes of carbon are present in either TEM or XRD. XPS from these films, however, did not detect any C (at detectability limit of ~0.1 at. %). Clearly, bulk covetic carbon structures cannot be transferred as-is to the thin film using e-beam evaporation. Since we could not obtain an accurate value of the C content (< 1 at. %) in the films we refer to the nominal concentration of the bulk Cu covetic target used for film deposition. Nevertheless, the presence of carbon in the copper matrix in the e-beam deposited films is evident by the improved properties compared to pure Cu films shown below.

Figure 3(a) shows the transmittance of Cu covetic and Cu metal films, measured at wavelengths ranging from 250 to 1100 nm. The peak at ~580 nm is due to the spectral nature of Cu. At this wavelength, the reflectance increases and absorbance decreases more significantly. Calculations by Ramirez-Porras and Vargas-Castro²¹ for copper suggest that at long wavelengths free carrier absorption dominates, but this effect decreases with wavelength due to screening by free carriers, which increases the reflectance (decrease in transmittance). At short wavelengths, reflectance is low and absorption dominates due to excitation of d-electrons into the conduction band. The combined effect gives rise to a crossover with a maximum at ~580 nm. This peak is also observed in the e-beam Cu cv 5% films. Remarkably, Cu cv 5% films are consistently more transparent than pure Cu films of the same thickness. Additionally, increasing the carbon content in the films increases transparency. Namely, a 20 nm film made by PLD from a nominally Cu cv 4% target has 1 wt. % (5 at. %) C content as measured by XPS (Figure 2(b)). This film exhibits ~90% transmittance over most of the wavelength tested (Figure 3(a)); a 40% increase over the 20 nm film made by e-beam deposition. The greater transparency in the covetic films may be due to the filling of interstitial sites in the Cu lattice resulting in a lower reflection coefficient. It is also possible that the additional electrons from the incorporation of carbon atoms in the covetic films raise the Fermi level, blocking the optical transition and increasing the transmittance.

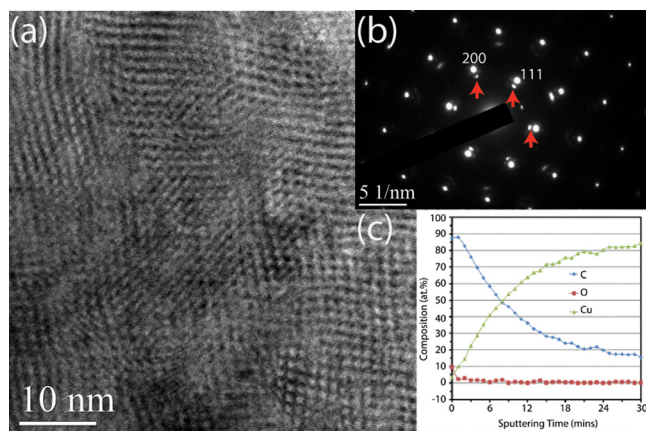


FIG. 1. (a) HRTEM image showing modulation due to the presence of nominally 5 wt. % C in the Cu covetic bulk, (b) the diffraction pattern from the area shown in (a). (c) XPS depth profile of Cu cv 5% bulk sample showing average C concentration of 15 at. % (~3.2 wt. %) after 24 min of sputtering.

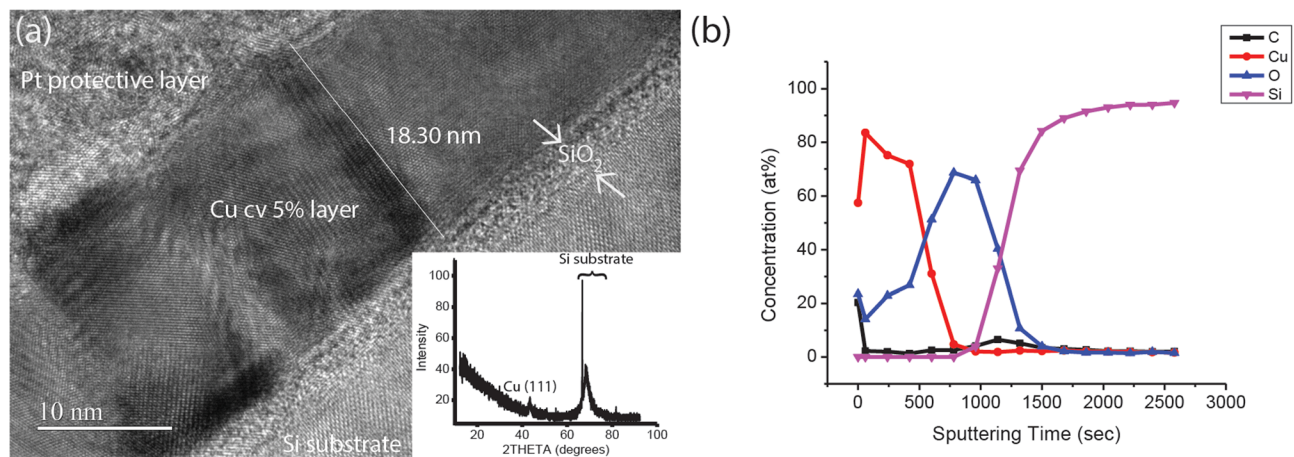


FIG. 2. (a) HRTEM image of an 18 nm thick Cu cv 5% film deposited by e-beam on Si. The inset is an XRD spectrum of the same film displaying a crystalline structure with Cu [111] texture and (b) XPS depth profiling of a 20 nm thick Cu cv 4% film grown by PLD on Si.

In order to ascertain the electrical properties and stability of the Cu and e-beam Cu covetic films, contacts were made by painting silver stripes onto the samples. The films were kept in air at room temperature and periodic measurements of the resistivity of the films were taken to assess the progression of the electrical properties with time. Covetic films show a perpetually lower resistivity than pure copper films of the same thickness (Figure 3(b)). The resistivity of the pure 10 and 20 nm Cu films degrades rapidly with time, while the 30 nm Cu film is stable over the time tested. The 20 and 30 nm covetic films are stable up to almost 80 days after deposition, but the resistivity of the 10 nm Cu covetic film increases fast with time although not as fast as the 10 nm Cu film. This is attributed to a 10% variation in thickness given by the RMS roughness of the 10 nm covetic film, which would significantly increase the surface area for oxidation and therefore degradation. The 20 and 30 nm Cu covetic films, in contrast, show very stable resistivity with time compared to the Cu films. The 20 nm covetic film also has relatively high transmittance above 50% at about 600 nm although it is lower for other wavelengths. The maximum transmittance of ~65% for the e-beam films was achieved in the 10 nm Cu covetic film, as shown in Figure 3(a). It is well known that nanostructures, such as graphene and CNTs,

have high electron mobility;²² however, highly conductive films formed from carbon nanostructures are obstructed by a high contact resistance at each CNT junction or through each graphitic plane.¹¹ Previous DFT calculations of the interface between graphene and metal substrates show that the electronic structure of graphene is preserved by weak adsorption on Cu substrates.^{23,24} In this work, we demonstrate the uniform integration of carbon nanostructures directly into the Cu lattice in Cu covetic. It is apparent that the high electron mobility of the graphitic structures that form in the Cu lattice enhances the charge transport in the covetic structure without being hindered by highly resistive sites typical of carbon nanostructure films.

For thin metal films, the relation between optical transmittance (T), and sheet resistance (R_s) can be modeled using the following equation:¹³

$$T = \left(1 + \frac{188\sigma_{opt}}{R_s\sigma_{dc}}\right)^{-2}. \quad (1)$$

The figure of merit is defined as the ratio (r) of the dc conductivity (σ_{dc}) and the optical conductivity (σ_{opt}). Cu covetic films demonstrate higher figure of merit than copper metal films, namely, $r = 59.05$ and 101.5 for the 10 nm Cu and Cu

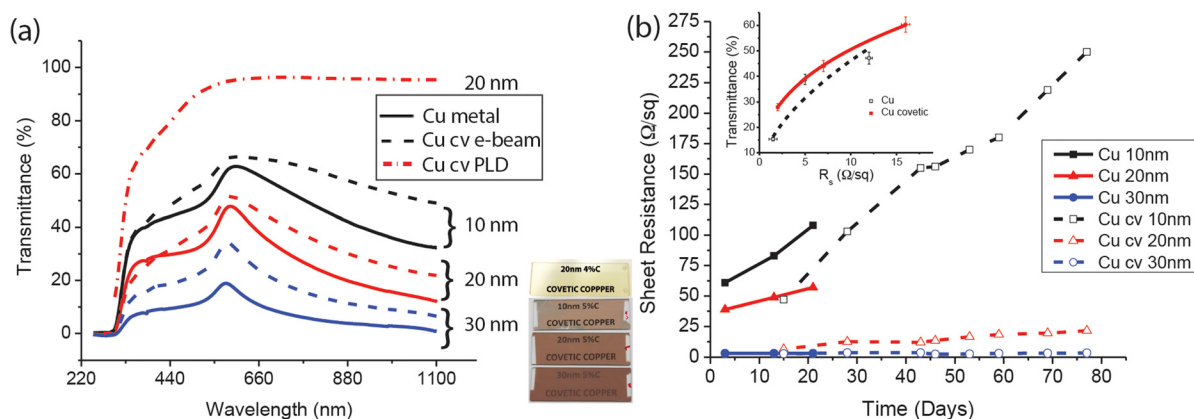


FIG. 3. (a) Transmittance measurement comparing Cu metal (0% C) with e-beam nominal Cu cv 5% films and PLD nominal 4% film. The inset in (a) shows optical images of the covetic films (top PLD film, bottom images e-beam films). (b) Stability measurement comparing the resistivity of Cu metal with Cu cv 5% films in air. The inset in (b) displays the transmittance vs sheet resistance of the e-beam covetic and Cu films measured at 550 nm.

covetic films, respectively (see inset to Fig. 3(b)). The electrical degradation of copper films with time is due to the formation of an insulating oxide layer on the film surface as has been observed in Al films that were exposed to air.²⁵ Tian *et al.*²⁶ have shown that the presence of graphene on a Cu surface can be an impenetrable barrier against oxidation. Unfortunately, the bonding between graphene and the copper surface is via van-der Waals forces and, consequently, it is very weak. In contrast, carbon in Cu covetic films provides resistance to oxidation by forming a network throughout the copper lattice with a strong bond between the carbon and the copper atoms. An oxide layer still develops on Cu covetic films, but with a slower rate than pure metal. We believe that the PLD films with higher carbon content are more resistant to oxidation than the e-beam films. The higher transmittance, decrease in resistance, and enhanced environmental stability demonstrate that Cu covetic is a promising material for transparent conducting electrodes.

The ampacity, maximum allowed current, of the 20 nm Cu and Cu covetic films was estimated using Eq. (2) derived by D'Amore *et al.*²⁷ for transparent metal films

$$I_L = \sqrt{\frac{2h(w + d_s)wd_s\sigma_s(T_s - T_e)}{1 + \alpha_s(T_s - T_e)}}, \quad (2)$$

where I_L is the film current-carrying limit, T_e is the environmental temperature surrounding the conductor, d_s , w , α_s , and σ_s are the film's thickness, width, temperature coefficient of resistance, and the electrical conductivity measured at T_e , respectively. The thermal limit is the maximum working temperature T_s , below which the film integrity is not compromised. The conductivities of a 20 nm Cu metal ($\sigma_{Cu} = 1.74 \times 10^7$ S/m) and Cu covetic ($\sigma_{covetic} = 1.77 \times 10^7$ S/m) films were obtained from the sheet resistance. The temperature coefficient of resistance of Cu is $\alpha_{Cu} = 3.94 \times 10^{-3} \text{ K}^{-1}$.²⁸ α was determined for Cu covetic (Cu cv 3%) bulk sample using a Physical Property Measurement System (Quantum Design) with a temperature range from 1.5 K to 350 K. At room temperature, $\alpha_{covetic} = 3.825 \times 10^{-3} \text{ K}^{-1}$. The coefficient h in Eq. (2) depends on factors including the thermal and dynamical properties of the fluid (air) and the geometrical configuration and heat absorption coefficient of the material sample.²⁷ In the case of natural convection, typical values of h range from 5 to 25 W/m²K. Figure 4 shows the current I_L of the films on glass as a function

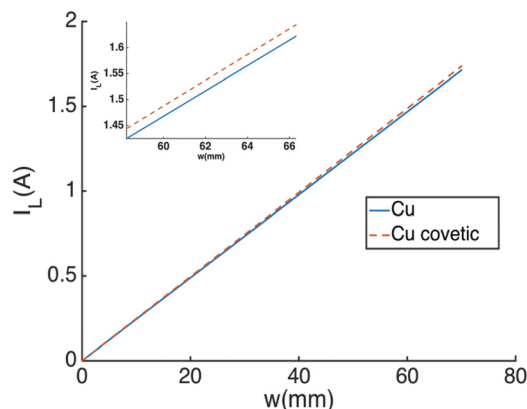


FIG. 4. Current at thermal limit as a function of the sample width for 20 nm films.

of sample width for $h = 10 \text{ W/m}^2\text{K}$, $d = 20 \text{ nm}$, $T_e = 20^\circ\text{C}$, and $T_s = 150^\circ\text{C}$. These data show that e-beam Cu cv 5% films have comparable or slightly higher ampacity than Cu metal films due to the presence of C in the film structure.

We have introduced copper covetic, a material that incorporates nanoscale carbon into the metallic structure of copper. Deposition of this material using e-beam deposition and PLD into a film on glass allows for the formation of a transparent conductor. Covetic films of comparable thickness have greater transparency, lower electrical resistivity, and greater stability when compared with pure copper films of the same thickness grown under the same conditions. e-beam copper covetic films of approximately 20 nm thick exhibit the best combination of electrical stability and transparency and show promise as a transparent conductive layer for many optoelectronic devices. We have also demonstrated that PLD films have higher C content in the film which gives rise to increased transparency. This work is a step forward in the development of a metal transparent conductor, which takes advantage of the high conductivity of copper, as well as nanocarbon species incorporated in the metal lattice. Future investigations on the effect of the carbon content on the properties of Cu covetic thin films are necessary to understand the role of carbon on the electrical and optical properties, as well as resistance to oxidation.

The copper covetic 5% bulk samples were provided by Third Millennium Materials, LLC in Waverly, Ohio. We acknowledge support from DARPA/ARL under Contract No. W911NF13100 and ONR Contract No. N000141410042 and the University of Maryland Faculty Incentives Program, the University of Maryland Nanocenter and the NISP lab. We thank the Center for Nanoscale Science and Technology at NIST for the use of the FIB/SEM.

¹D. S. Hecht, L. Hu, and G. Irvin, *Adv. Mater.* **23**, 1482 (2011).

²L. Hu, H. Wu, and Y. Cui, *MRS Bull.* **36**, 760 (2011).

³J.-Y. Lee, S. T. Connor, Y. Cui, and P. Peumans, *Nano Lett.* **8**, 689 (2008).

⁴J. H. Lee, P. Lee, D. Lee, S. S. Lee, and S. H. Ko, *Cryst. Growth Des.* **12**, 5598 (2012).

⁵S. De, T. M. Higgins, P. E. Lyons, E. M. Doherty, P. N. Nirmalraj, W. J. Blau, J. J. Boland, and J. N. Coleman, *ACS Nano* **3**, 1767 (2009).

⁶A. Sánchez-Iglesias, B. Rivas-Murias, M. Grzelczak, J. Pérez-Juste, L. M. Liz-Marzán, F. Rivadulla, and M. A. Correa-Duarte, *Nano Lett.* **12**, 6066 (2012).

⁷P. E. Lyons, S. De, J. Elias, M. Schamel, L. Philippe, A. T. Bellew, J. J. Boland, and J. N. Coleman, *J. Phys. Chem. Lett.* **2**, 3058 (2011).

⁸H. Guo, N. Lin, Y. Chen, Z. Wang, Q. Xie, T. Zheng, N. Gao, S. Li, J. Kang, D. Cai, and D.-L. Peng, *Sci. Rep.* **3**, 2323 (2013).

⁹A. R. Rathmell, S. M. Bergin, Y.-L. Hua, Z.-Y. Li, and B. J. Wiley, *Adv. Mater.* **22**, 3558 (2010).

¹⁰S. Bae, H. Kim, Y. Lee, X. Xu, J.-S. Park, Y. Zheng, J. Balakrishnan, T. Lei, H. R. Kim, Y. Il Song, Y.-J. Kim, K. S. Kim, B. Ozyilmaz, J.-H. Ahn, B. H. Hong, and S. Iijima, *Nat. Nanotechnol.* **5**, 574 (2010).

¹¹H. Wu, L. Hu, M. W. Rowell, D. Kong, J. J. Cha, J. R. McDonough, J. Zhu, Y. Yang, M. D. McGehee, and Y. Cui, *Nano Lett.* **10**, 4242 (2010).

¹²H. Wu, D. Kong, Z. Ruan, P.-C. Hsu, S. Wang, Z. Yu, T. J. Carney, L. Hu, S. Fan, and Y. Cui, *Nat. Nanotechnol.* **8**, 421 (2013).

¹³Y. Zhou, L. Hu, and G. Gruner, *Appl. Phys. Lett.* **88**, 123109 (2006).

¹⁴A. R. Rathmell, M. Nguyen, M. Chi, and B. J. Wiley, *Nano Lett.* **12**, 3193 (2012).

¹⁵P.-C. Hsu, H. Wu, T. J. Carney, M. T. McDowell, Y. Yang, E. C. Garnett, M. Li, L. Hu, and Y. Cui, *ACS Nano* **6**, 5150 (2012).

¹⁶J. Shugart and R. Scherer, U.S. patent 2013062572 A2 (2013).

¹⁷T. Knych, P. Kwaśniewski, G. Kiesiewicz, A. Mamala, A. Kawecki, and B. Smyrak, *Metall. Mater. Trans. B* **45**, 1196 (2014).

- ¹⁸J. E. Cornett and O. Rabin, *Solid State Electron.* **101**, 106 (2014).
- ¹⁹J. A. Rodríguez-Manzo, M. Terrones, H. Terrones, H. W. Kroto, L. Sun, and F. Banhart, *Nat. Nanotechnol.* **2**, 307 (2007).
- ²⁰A. V. Krasheninnikov and F. Banhart, *Nat. Mater.* **6**, 723 (2007).
- ²¹A. Ramirez-Porras and W. E. Vargas-Castro, *Appl. Opt.* **43**, 1508 (2004).
- ²²A. K. Geim, *Science* **324**, 1530 (2009).
- ²³G. Giovannetti, P. Khomyakov, G. Brocks, V. Karpan, J. van den Brink, and P. Kelly, *Phys. Rev. Lett.* **101**, 026803 (2008).
- ²⁴Z. Xu and M. J. Buehler, *J. Phys. Condens. Matter* **22**, 485301 (2010).
- ²⁵J. M. Camacho and A. I. Oliva, *Thin Solid Films* **515**, 1881 (2006).
- ²⁶J. Tian, H. Cao, W. Wu, Q. Yu, N. P. Guisinger, and Y. P. Chen, *Nano Lett.* **12**, 3893 (2012).
- ²⁷M. D'Amore, M. S. Sarto, A. Tamburrano, and F. Sarto, *IEEE Int. Symp. Electromagn. Compat.* **3**, 900 (2005).
- ²⁸J. H. Dellingner, *The Temperature Coefficient of Resistance of Copper* (National Bureau of Standards, 1911).